geosciences

MDPI

Article

Exploring Imaging Methods for In Situ Measurements of the Visual Appearance of Snow

Mathieu Nguyen [1,*], Jean-Baptiste Thomas [1,2] and Ivar Farup [1]

[1] Colourlab, Department of Computer Science, Norwegian University of Science and Technology (NTNU), 2815 Gjøvik, Norway; jean.b.thomas@ntnu.no (J.-B.T.); ivar.farup@ntnu.no (I.F.)
[2] Imagerie et Vision Artificielle (ImVIA) Laboratory, Department Informatique, Electronique, Mécanique (IEM), Université de Bourgogne, 21000 Dijon, France
* Correspondence: mathieu.nguyen@ntnu.no

Abstract: We explored imaging methods to perform in situ field measurements of physical correlates of the visual appearance of snow. Measurements were performed at three locations in Norway between February and March 2023. We used a method to estimate the absorption and scattering coefficients of snow using only one measurement of reflectance captured by the Dia-Stron© TLS850 translucency meter. We also measured the sparkle indicators (contrast and density of sparkle spots) from digital images of snow. The contrast of sparkle spots can be defined as the median value of all the pixels identified as sparkle spots by an algorithm, and the density of sparkle spots is the number of sparkle spots in a selected area of the image. In the case of the sparkle of the snow surface, we found that there is a potential to use the sparkle indicators for classifying the grain types, but it requires a larger data set coupled with expert labelling to define the type of snow. For the absorption and scattering properties, the measurements confirm the fact that snow is a weakly absorptive and highly scattering material when modelling light interactions in the snow. No correlation between the optical properties and sparkle could be found in our data.

Keywords: visual appearance; snow; outdoor in situ measurements; sparkle; absorption; scattering; imaging methods

Citation: Nguyen, M.; Thomas, J.-B.; Farup, I. Exploring Imaging Methods for In Situ Measurements of the Visual Appearance of Snow. *Geosciences* **2024**, *14*, 35. https://doi.org/10.3390/geosciences14020035

Academic Editors: Ulrich Kamp and Jesus Martinez-Frias

Received: 15 December 2023
Revised: 24 January 2024
Accepted: 27 January 2024
Published: 29 January 2024

1. Introduction

Snow is usually known as a uniform white and cold surface observable during winter or in specific environments, but its surface can present a bluish colour aspect due to internal scattering [1,2]. It is also known as a material with high albedo [3,4]. Four aspects are used to describe the visual appearance of a material: colour, gloss, texture, and translucency [5]. However, the visual appearance of snow is not limited to these four aspects but can be linked to other parameters of snow itself [6]. Snow layers are composed of snow grains, usually characterised by their size and shape [7,8]. Classifications have been carried out to collect various sizes and shapes of snow depending on weather conditions, which can help identify their properties [6]. There have also been several studies examining the albedo of snow in relation to its metamorphism [9] or using remote sensing satellite technologies to perform measurements [10,11] instead of in situ measurements [12].

Translucency models and methods used to capture the properties of snow were discussed by Frisvad et al. [13]. These can be linked to two optical properties of the material: the absorption and the scattering coefficients. These coefficients can naturally be connected with models aimed at solving the Radiative Transfer Equation (RTE) [14], which describes how light propagates inside a material. Such models are called Bidirectional Reflectance Distribution Function (BRDF) [15] models, and several methods exist to capture these functions for various applications [16]. In the case of snow, radiative transfer models representing the BRDF of snow have recently been developed [7,17]. The model introduced by

Kokhanovsky and Zege provides a correlation between the reflectance function and parameters related to snow layers, specifically snow grain size and snow grain shape. This model has been used in the literature to estimate these parameters [18,19]. Extensions of the BRDF can also be found, such as the Bidirectional Subsurface Scattering Reflectance Distribution Function (BSSRDF), which contains information about the surface reflectance of a material and adds the contribution of light scattering occurring under the subsurface [20]. This BSSRDF is impractical to measure, as it requires estimates of the absorption and scattering coefficients of the material, but it is mainly used for computer graphics rendering [13,21]. Studies on the absorption properties of snow have also been conducted [22]. Warren et al. presented a database of imaginary values for the complex refractive index of snow and ice that goes from the ultraviolet (100–400 nm) to the microwave. Later on, this database was refined to obtain accurate values [23,24].

There is already knowledge of the absorption coefficient [22], but very few studies exist on the scattering values for snow. A method was developed to estimate these coefficients in the case of highly diffuse materials [25], and the advantage of this study is that it only needs one measurement of the reflectance profile at the contact of the material. Another feature of the visual appearance of snow can be linked to a texture effect, such as sparkle. Once formed, snow grains act similarly to microflakes and can produce sparkle by reflecting incoming directional light, similar to tiny mirrors [26]. A statistical study of the sparkle of snow was conducted on digital images [27] by adapting the measurement method of sparkle designed by Ferrero et al. [28]. Ultimately, absorption, scattering, and sparkle can all be connected to snow grains. The aforementioned imaging methods are all compatible with outdoor in situ measurements. Acquiring data on snow inside a laboratory is possible [29,30], but in situ measurements allow the snow to remain close to its natural state without disrupting its evolution and are thus preferred [12,31].

Within the study detailed in this paper, we explore the methods we have previously designed and validated to connect with sparkle and the optical properties of snow. In the case of the sparkle of snow, our goal is to verify the previous results we obtained and check whether we can reproduce these results with a new set of snow images with visible sparkle. For the optical properties, that is, the absorption and scattering coefficients, we utilise the developed inversion method to obtain estimates and validate them with values from the literature. Furthermore, we investigate whether these physical correlates of visual appearance present a time variation with evolving snow due to changes in temperature or new fallen snow. In the case of both parameters, we focus on the visible range (400 to 800 nm); however, this could be extended to other parts of the spectrum with adequate materials and methods.

2. Methods

The following sections present the imaging methods used for each studied parameter. The processing pipelines of these methods are illustrated in Figure 1.

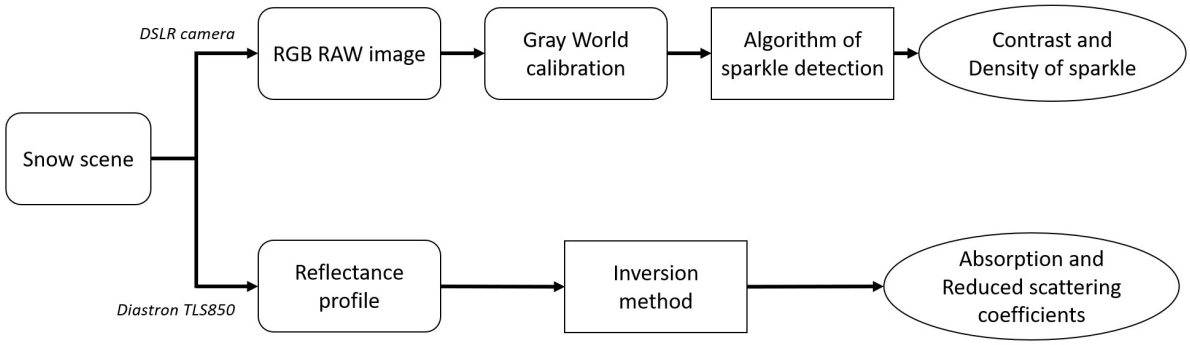

Figure 1. Acquisition and processing pipelines used in this study. The top path corresponds to the method for studying the sparkle of snow, whereas the bottom path is followed to obtain estimates of the absorption and scattering properties of snow.

2.1. Sparkle of Snow

The algorithm to detect sparkle from digital images was adapted from the general work by Ferrero et al. [28], and the special case of the sparkle of snow was introduced in one of our previous works [27]. We used the same algorithm from this previous work to measure the sparkle of the snow surface from digital images. The images we used for this study were new, and we performed small changes to the capture process, which we explain later. We performed our in situ data collection in Norway at three snow sites between February and March 2023. The three sites selected were the same across all measurements to ensure consistency and a point of comparison. We monitored changes in the measured parameters due to changes in temperature and new fallen snow.

Running the sparkle detection algorithm requires snow images with visible sparkle. The images were captured using a DSLR Nikon D610 camera with an adjustable lens. The camera has a CMOS sensor with a size of 35.9 × 24 mm, providing images with a resolution of 6048 × 4016 pixels. The camera was held by a user at their height and was not fixed on a tripod. All sparkle images were taken under directional sunlight with a cloudless sky to optimise the visibility of sparkle and reduce the possibility of observing graininess that would occur under diffuse illumination [26]. Graininess is the aspect of observing granular particles. Examples of such images are shown in Figure 2, and it is possible to observe some graininess in some of them. Due to the time zone and time of year, the images were acquired between 10 a.m. and 12 p.m. CET (Central European Time). For each snow scene, images were taken by focusing on an area of interest in the frame, and then rotating around that zone. With this method, we aimed to obtain images of the same area but with varying views and illumination angles, and thus investigate whether the indicators of sparkle would be affected by these rotations. Several focal lengths were utilised to capture the images, ranging from 50 mm to 300 mm (see Figure 3).

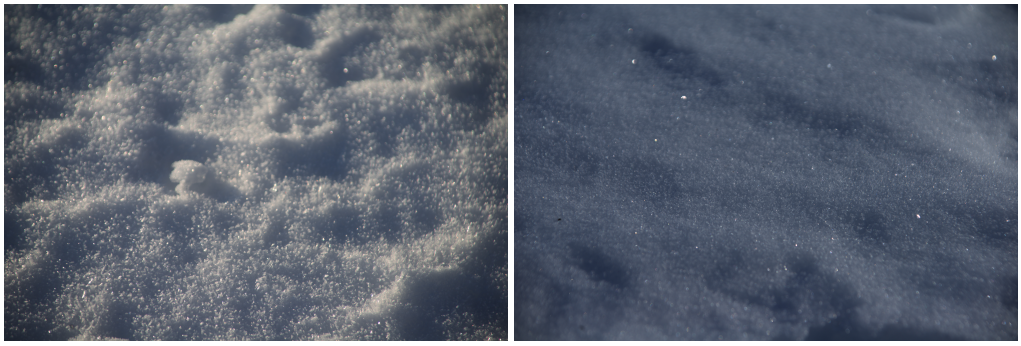

Figure 2. Snow images taken during our field campaign. (**left**) Snow image with visible sparkle. (**right**) Snow image with visible sparkle and a bit of graininess.

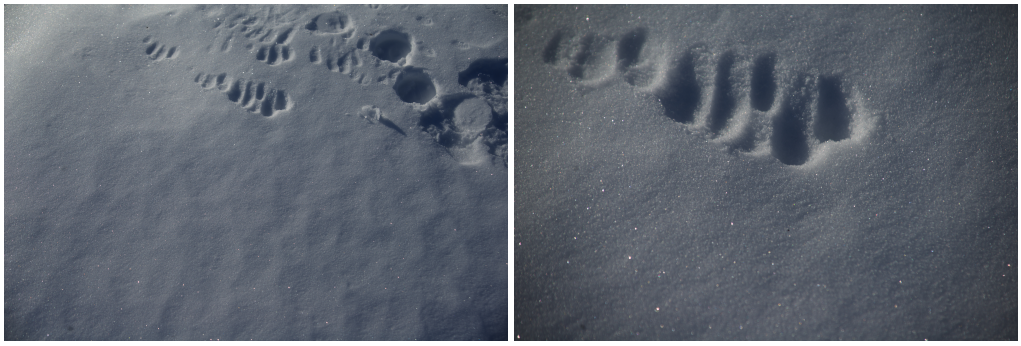

Figure 3. Examples of snow images with sparkle taken with different focal lengths. (**left**) Picture taken with 60 mm focal length. (**right**) Picture taken with 300 mm focal length.

In total, we acquired 1033 images. In addition, we captured images with the camera at grazing angles (elevation angle close to 90°, close to the surface) to accentuate the sparkle

phenomenon produced by natural light. For each set, we focused on one area, and then the camera was slightly moved with small horizontal or vertical translations. We consider these images as a different set, and with them, we aim to establish an uncertainty scale of the sparkle indicators, the contrast, and the density of sparkle spots. The contrast of sparkle spots can be defined as the median value of all the pixels identified as sparkle spots by the algorithm. The density of sparkle spots would thus be the number of sparkle spots in a given area in the image. More details on their definitions can be found in our previous study [27].

2.2. Absorption and Scattering of Snow

To obtain estimates of the absorption and scattering coefficients of snow, we utilised a translucency meter device called the © Dia-Stron TLS850. We had previous knowledge of this particular device from our work on estimations of the optical properties of highly diffuse materials. This device comprises three RGB LEDs coupled with an NMOS sensor and allows for the measurement of the reflectance profiles of a material. The wavelengths available with the LEDs are 630, 525, and 472 nm. Specifically, as the device needs to be in contact with the surface of the material, it is possible to emit and capture the light scattered under the surface. A description of the device can be found in our previous paper [25].

Following a similar pattern to the method used for sparkle images, we acquired our data using the TLS device in situ for the same three snow scenes. The setup consisted of the translucency meter device, an external battery, and a laptop (see Figure 4). The TLS is practical, as its ergonomic design allows us to perform acquisitions outside, as long as one owns a battery to plug the device into. During our preliminary tests and field measurements, the device did not emit warmth from its use that could damage the structure of the snow. As mentioned, the device is handheld and needs to be put in contact with the material surface. In the case of snow, it is important to maintain contact but not let the natural weight of the sensor exert excessive force; otherwise, it could compress the snow and affect its structure. We noticed this effect during our preliminary test, and we managed to avoid it during the field measurements so as not to change the grain structure. Moreover, the device is plugged into a laptop via a USB cable and acquisitions are piloted using the device software. As shown in Figure 4, the protocol used is impractical for one person to perform.

Figure 4. In situ setup to acquire reflectance profiles using the TLS850 for one of the three snow scenes.

An additional component that should be mentioned in the acquisition protocol for the optical properties of snow is illumination. The TLS device generates illumination for reflectance, as it uses LEDs to illuminate the sample with three wavelengths: 630, 525, and 472 nm. However, due to the sensitivity of its sensor and the high diffusion of the snow

material, conducting these measurements under sunlight could create noise and saturation in the reflectance profiles. Noise can be smoothed, but the light diffused from the snow material around the area of acquisition can introduce bias to the signal. Without having precise knowledge of this bias, correcting the offset would be difficult. Thus, even though the image shown in Figure 4 was shot in daylight for illustrative purposes, all acquisitions were realised at night to reduce the effects of added bias and ambient light around the area of acquisition.

Finally, to estimate the absorption and scattering coefficients, we used the inversion method introduced in [25], for which certain constraints need to be satisfied. These constraints are that the material should be highly diffuse with low absorption, and it should satisfy the semi-infinite assumption. Let us verify whether snow meets these constraints. First, snow is characterised as a material with low absorption properties and a dominance of scattering, as shown by the values of the imaginary part of the complex refractive index [23,24]. So, snow is a highly diffuse material. Furthermore, to use the inversion method to fit the reflectance profiles to the diffusion theory model [20,32], providing an asymptotic solution to the RTE, the material considered has to satisfy the semi-infinite assumption. In the case of snow, this assumption states that the snow thickness must be large enough compared to the wavelength considered, and its vertical dimensions must be large enough compared to the sensor size. Previous studies have used this assumption to simplify the equations of their models and solve the RTE [7,18,31]. Therefore, snow is a low-absorptive and highly scattering material, which satisfies the semi-infinite assumption. The constraints for using the inversion method have been verified.

2.3. Field Acquisition Campaign

Studies on snow are seasonal and dependent on the amount of snow one has access to, as in situ studies can be sparse and rare and are often replaced with satellite observations [11,12]. For this work, all field measurements related to the sparkle of snow and the optical properties of snow were obtained between 9 February (labelled as day 1) and 23 March (day 43). In total, we collected sparkle data on 14 days and optical properties data on 14 days as well. Although these days were not the same, there were overlapping days. Specific weather conditions were required for data collection. In the case of sparkle, a sky without clouds and directional sunlight is needed. Clouds could be a source of diffuse light, which is not recommended for observing sparkle [26]. For the absorption and scattering properties, we collected the data at night, and we tried as much as possible to collect data on the same days we collected sparkle, even though several structural changes can occur in one day. Furthermore, reflectance profiles cannot be acquired under snowfall, as it could damage the setup, which is shown in Figure 4. Eventually, for these 42 measurement days, we were able to observe different types of snow, as there were changes in the temperature and snowfalls, which added new layers of fresher snow. We compiled three categories for the types of snow based only on our observations, as shown in Table 1: fresh snow (F) for when there had been snowfall, dense snow (D) for when the snow had accumulated for some time without new snow and temperatures were cold enough, and old snow (O) for snow whose melting process had started. In this article, we use customised snow labels, as we did not precisely measure the parameters of snow that would allow us to have a precise classification of snow. An example of this can be found in the report by Fierz et al. [6], as they classified snow based on metrics such as snow grain sizes or grain shapes.

Table 1. Snow labels for each acquisition. (F) Fresh snow, (D) dense snow, and (O) old snow. We also report the focal lengths f' we used to capture snow images with sparkle. Days marked with an "-" for focal lengths correspond to days without sparkle measurements.

Day	**1**	**5**	**6**	**12**
Label	D	D	D	F
f' (mm)	50/65/300	50/60/300	55/70/300	50/300
Day	**13**	**15**	**17**	**19**
Label	F	F	D	D
f' (mm)	50/65/300	-	-	55/300
Day	**20**	**21**	**22**	**23**
Label	D	D	D	D
f' (mm)	60/70/85/300	60/70/300	-	-
Day	**26**	**27**	**29**	**30**
Label	D	D	O	O
f' (mm)	60/70/92/300	55/60/65/300	50/70/300	55/60/300
Day	**34**	**35**	**43**	
Label	F	F	O	
f' (mm)	-	50/65/30	65/70/300	

Furthermore, Figure 5 shows the temperature data for each day of field measurements. This allows for monitoring the average temperature of each day and the minimum and maximum values achieved. One could potentially estimate the gradient of temperature that the snow experienced at various resolutions (daily or hourly), although we do not compute it in this study.

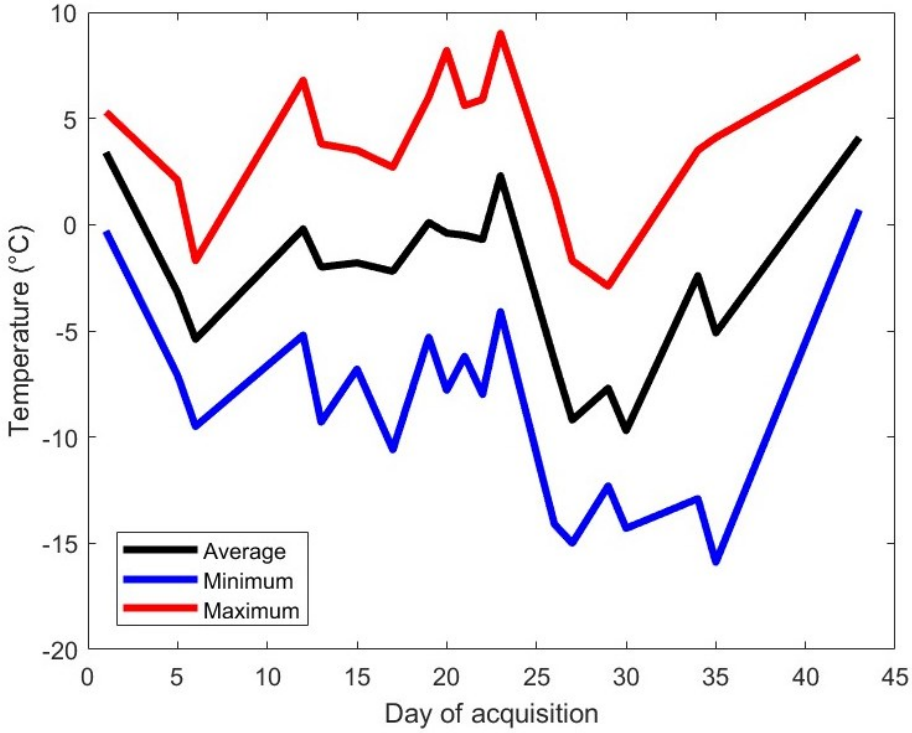

Figure 5. Tracking of temperatures on the measurement days. Data recorded include the average temperature for each day, as well as the minimum and maximum values, to provide an idea of the amplitude. Temperature data were collected from the website yr.no [33], which uses local sensors from measuring stations near the field site locations (within a range of less than 10 km).

The data generated in this study include the contrast and density values of sparkle spots, the values of the absorption and reduced scattering coefficients, and the temperatures

recorded with daily and hourly resolution for each day of the field measurements. All of these data have been made publicly available.

3. Analysis and Discussion

3.1. Study of Sparkle

Two indicators are mainly used to characterise the sparkle of snow estimated from the digital images [27]. The contrast of the sparkle spots describes the maximum value of the luminance factor between the sparkle pixels and the background pixels. It characterises the intensity of the sparkle spots on the images. The density of the sparkle spots is related to the number of sparkle spots counted by the algorithm in the region of interest delimited in the image. Only sparkle spots above a certain threshold are considered for this quantity. Thus, a good way to characterise the images we collected with visible sparkle is to compute these indicators for all images acquired during the 14 days for the three snow scenes.

Figure 6 shows the results of the contrast values for our dataset. One can see that there are cases where the boxes are minuscule because the contrast values are almost similar. One point of note is that there is a decreasing trend in the median contrast values for days 1 to 13. These values increase on day 19 and then decrease again until the end of our field measurements. This could be correlated with a change in the type of snow (as shown in Table 1), but could also be related to a change in temperature, as shown in Figure 5. When focusing on the density indicators in Figure 7, although we can observe high variability among the data with a large spread for the average values, there is no variation observed, as is the case for the contrast values. The temperature has an effect on the snow's metamorphism and, therefore, the grain type [6]. Due to positive temperatures, snow grains grow larger in melt metamorphism. Due to the ensuing cold temperatures, the melted water refreezes, and the newly formed snow surface may reflect light with a higher intensity. As a consequence, the detected sparkle would be more intense, thus explaining the increase in the contrast values.

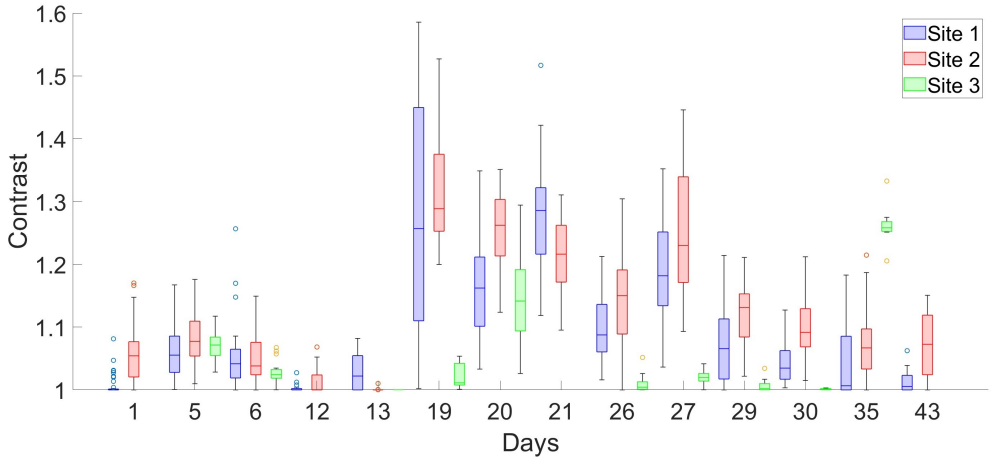

Figure 6. Box plots illustrating the computed contrast values of the sparkle indicator for the three snow sites. The top and bottom edges of the boxes represent the lower and upper quartiles of the data, respectively, whereas the lines within the boxes indicate the median values. The endpoints of the lines outside the boxes indicate the maximum and minimum values of the data for the day. Circles on some days are values outside of the range of boxes.

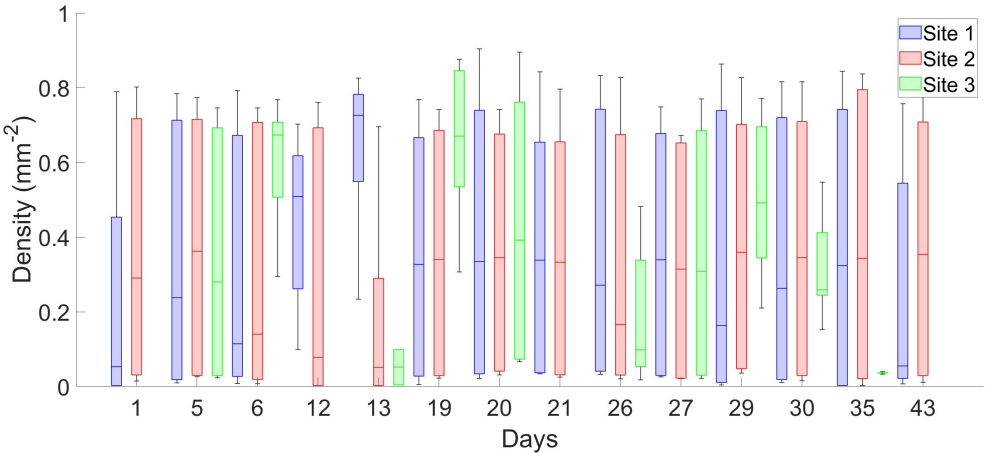

Figure 7. Box plots illustrating the computed density of the sparkle indicator for the three snow sites. The top and bottom edges of the boxes represent the lower and upper quartiles of the data, respectively, whereas the lines within the boxes indicate the median values. The endpoints of the lines outside the boxes indicate the maximum and minimum values of the data for the day.

Similar to our previous study [27], we utilised a plot to illustrate the relationship between the contrast and density indicators, as shown in Figure 8. We can clearly observe two distinct clusters in the values, with some density values being very low and others slightly higher. We used a k-means clustering algorithm with $k = 2$ to show the two clusters. When looking at the data of the images, we found one varying parameter that could explain the clustering of values: the change in the focal length during image capture. In Figure 8, the red region corresponds to values obtained from images taken with focal lengths in the range of 50 to 85 mm, whereas the blue region represents values from images taken with a focal length of 300 mm. During the campaign, images were acquired with different focal lengths because we wanted to experiment with various setups, with some being more close-up than others. So, we obtained images for which the zoom was more important than others, resulting in larger snow grains and making sparkle detection easier for the algorithm to detect. Thus, the covered area differs for some images, but we ensured an overlapping area in all images from the same site. The focal length of each image can be found in the metadata of the RAW image. As can be seen in Figure 3, there is a significant difference in the potential area that can be covered for detecting sparkle. This raises questions about the ground resolution and depth of field that need to be chosen for the algorithm to effectively detect sparkle spots. Although it is possible for a human observer to see sparkle on images with focal lengths less than 100 mm, the algorithm may behave differently. The resolution to achieve from an imaging point of view needs to be further refined and may need to be adapted to each case studied. Images in this dataset were acquired by an observer from their height, and thus the distance between the camera and the snow material varies between 1.8 and 2 m. At these distances, a higher focal length seems to be required in order to observe sparkle in images. For future investigations, one should consider having a fixed distance for capturing images with sparkle, in accordance with the desired ground resolution.

We also recorded several image sets for which images were taken by focusing on one area of interest with visible sparkle, and then small vertical or horizontal movements were made around this region. The aim was to slightly change the viewing angle of the scene to potentially observe different sparkle events in the same neighbourhood. Unlike the previous images, these images were captured in a close-up setting by an observer trying to get close to the material. The distance between the camera and the area of snow was less than one meter. So, the focal lengths were adapted to observe imaging sparkle. Table 2 presents the results of the sparkle indicators computed for these images, with their mean values and standard deviations. For sets 2, 6, and 7, the contrast values are low and close

to 1, indicating that the intensity of sparkle was almost uniform, and there were no shiny spots in the snow, whereas the density values for sets 2 and 7 are high with significant variability. Set 4 exhibits contrast values with a high standard deviation. When focusing on the images in this set, several sparkle spots and even some visible snow crystals can be seen. This may have led to the detection of higher contrast values by the algorithm. Moreover, set 4 was acquired with a focal length of 170 mm, which is higher than the other image sets, as they were captured with focal lengths less than 100 mm. This explains why snow crystals were visible and why the sparkle spots were more intense, resulting in the high variability of the contrast values. This again highlights the fact that the settings of the camera and the chosen resolution have a major influence on the results of the study of sparkle.

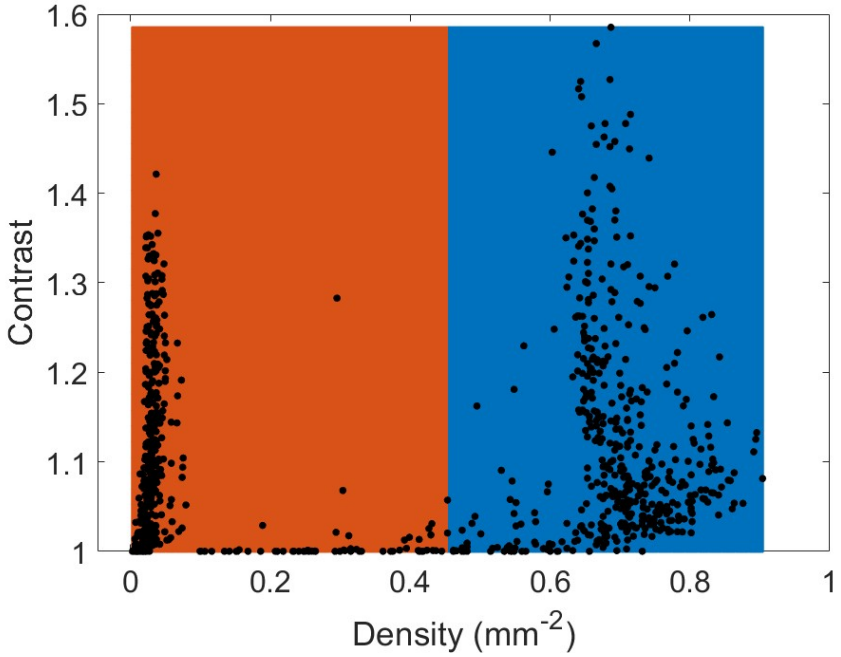

Figure 8. Plotting contrast values (black dots) versus density values for the entire dataset consisting of 1033 images. We used a *k*-means clustering method with $k = 2$ to categorise our results. The red region corresponds to images captured with a focal length between 50 and 92 mm, whereas the blue region corresponds to images captured with a focal length of 300 mm.

Table 2. Contrast and density results, including their means and standard deviations, for image sets captured by focusing on one area with small horizontal or vertical movements around this position.

Set	Contrast		Density (mm^{-2})	
	Mean	Std	Mean	Std
1	1.3368	0.0687	0.0619	0.0022
2	1.0300	0.0425	0.5436	0.2365
3	1.2082	0.0337	0.0803	0.0028
4	1.4551	1.1278	0.1914	0.0905
5	1.2735	0.0472	0.1229	0.0021
6	1.0043	0.0068	0.0211	0.0108
7	1.0021	0.0051	0.3169	0.1376

One of the conclusions from our previous study [27] was that sparkle could potentially be used as an indicator to classify snow, as we observed specific variations in the contrast and density values for the three types of snow introduced (fresh, dense, and old snow). Using the nomenclature of Table 1 and a classification algorithm, it may be possible to check the validity of this conclusion. We utilised the multiclass learning ECOC classifier provided

by ©Matlab (Error-Correcting Output Codes) to perform the classification using the three labels we assigned to each day of acquisition. Then, we computed the resubstitution classification error to determine how well the classifier has learned based on the data provided, obtaining a classification error of 38.4%. Although this error value does not allow for a conclusive classification of snow with sparkle, as shown in [27], there is potential. Some reasons we were unable to reproduce the results with this current dataset could be linked to the acquisition protocol. Although we used the same DSLR camera, we did not use a tripod this time, and we chose to turn around one point in the scenes to obtain more pictures. Furthermore, the labels assigned to the snow types are not the most accurate possible and they were chosen solely through empirical observation (without the use of any metrics). This classification could be improved by obtaining values of snow grain sizes through digital measurements [10,34]. Although the sparkle indicators computed for this current dataset do not allow for a conclusive classification, this can be attributed to this specific set of images for this type of snow. Repeating this procedure across several datasets and on different types of snow in various locations would be ideal in order to confirm this theory.

3.2. Study of Absorption and Scattering Coefficients

The second part of this study focuses on the absorption and scattering coefficients of snow, which can be estimated using the method developed in [25]. Regarding the absorption coefficient of snow, several studies have been conducted in recent years [22–24]. From the electromagnetic theory, it is possible to link the absorption coefficient of a medium μ_a to the imaginary part m_I of its complex refractive index and the wavelength λ of the electromagnetic wave considered in Equation (1).

$$\mu_a = \frac{4\pi m_I}{\lambda} \tag{1}$$

The estimation method we designed is based on a nonlinear least-squares inversion method and currently includes two unknown parameters: the absorption, μ_a, and reduced scattering, μ_s', coefficients. First, we compared the μ_a estimated using our method with the theoretical values calculated using Equation (1), and the database of Picard et al. [23] for the m_I values. These estimated values are presented in Table 3.

Table 3. Estimated values of absorption coefficients from in situ measurements of snow. The theoretical values of μ_a for RGB are (2.07×10^{-4}, 5.74×10^{-5}, 4.17×10^{-5}) mm^{-1}.

Day	μ_a (mm^{-1})		
	R	**G**	**B**
12	1.74×10^{-4}	2.07×10^{-4}	1.50×10^{-4}
13	3.06×10^{-4}	2.95×10^{-4}	4.30×10^{-4}
15	1.10×10^{-4}	2.06×10^{-4}	2.52×10^{-4}
17	5.99×10^{-5}	7.94×10^{-5}	2.26×10^{-4}
19	6.81×10^{-4}	4.30×10^{-4}	4.50×10^{-4}
20	6.54×10^{-4}	7.20×10^{-4}	6.57×10^{-4}
21	2.69×10^{-4}	3.35×10^{-4}	3.88×10^{-4}
22	8.90×10^{-4}	9.88×10^{-4}	2.90×10^{-3}
23	1.30×10^{-4}	2.36×10^{-4}	2.20×10^{-4}
26	2.66×10^{-5}	3.00×10^{-5}	4.56×10^{-5}
27	1.72×10^{-4}	1.20×10^{-4}	5.50×10^{-5}
29	1.72×10^{-4}	1.91×10^{-4}	2.22×10^{-4}
30	9.20×10^{-5}	1.40×10^{-4}	9.09×10^{-5}
34	1.30×10^{-2}	5.10×10^{-3}	1.30×10^{-3}

As seen in Table 3, the data estimated on day 34 seem to be overestimated. But even when not considering this day, all the other values are higher than the theoretical values,

with very few of them falling within a confidence interval of 10%. This was expected, as one of the limitations of the method discussed in [25] is that, due to materials with low absorption properties, the accurate estimation of the absorption coefficients becomes more difficult. The method was validated on other highly diffuse materials, such as milk, in our previous study [25]. Even with these previous results, obtaining correct results for the snow in that area was not guaranteed. However, this does not mean that these results should not be trusted to a certain degree. The database of complex refractive indices for ice, which was then extended to snow by Warren et al. [22,24] and Picard et al. [23], was established with one specific type of pure snow. Our results were obtained from evolving snow, so there could be differences in the way the snow material absorbs light.

Snow remains a weakly absorptive material [7]. Although there are differences between our estimates of the absorption coefficient and the theoretical values, this could be neglected, as scattering is the dominant phenomenon in snow. As mentioned, our original inversion method gives estimates of μ_a and μ_s' from the reflectance profiles acquired with the TLS device, labelled as Method 1. However, in the case of snow, since the theoretical values of μ_a can be computed individually for each wavelength, the number of unknowns in the inversion problem can be reduced from 2 to 1, thus simplifying the solution. We implemented this version, for which we only estimated μ_s' from the TLS data, with μ_a as prior values, labelled as Method 2. The results from these two methods are displayed in Table 4. Except for day 23, one trend that can be observed is that the scattering coefficients for the green channel are larger than those for blue and red channels, which means that snow scatters more green wavelengths. This was unexpected, as usually, snow has a tendency to exhibit colour towards the blue region [1] and stronger values of scattering would be expected in that region. However, the differences between the estimated values of the green and blue channels are not large. When comparing the results of both methods, the relative differences between Method 1 and Method 2 are 4.32% for the red channel, 4.71% for the green channel, and 4.10% for the blue channel. These differences are acceptable, and the choice is left regarding which method to choose when estimating these scattering properties. Finally, another aspect we can look into with the reduced scattering coefficients is the potential classification of snow. As we can observe from the results in Tables 3 and 4, there are variations on each day of acquisition. As there are changes in temperature and new fallen snow accumulating in the area of acquisition, these variations are coherent. The question that remains is whether we could use them to identify the type of snow. Using the same nomenclature as specified in Table 1 and the ECOC classification provided by ©Matlab, the computed error of classification with the estimated reduced scattering coefficients is 42.86% for both Methods 1 and 2. This error value does not allow for a conclusive classification of snow based on the scattering coefficient. Similar to the sparkle study, our labelling may be questioned, as it was done empirically and solely based on visual characteristics. However, it could also be that optical properties are not discriminatory enough to characterise a constantly evolving material like snow.

A common application of the knowledge of absorption and scattering coefficients is that it gives a description of the BSSRDF of the material studied [21]. The dipole model [20] was implemented to represent the contribution of subsurface scattering through these coefficients. Therefore, once the knowledge of these parameters is known, it is possible to produce rendered images. The physically based renderer Mitsuba 3, designed by Jakob et al. [35], can be used to implement rendering materials with subsurface scattering. Using the estimated values of the absorption and reduced scattering coefficients for day 21 from Tables 3 and 4 and a 3D object modelled on one of the snow scenes surveyed for data during our campaign, we were able to render images. The 3D object was obtained by scanning the scene using a LiDAR scanner embedded in a smartphone. With such images, one could use them to qualitatively verify whether the estimated values of the absorption and reduced scattering coefficients are correct or if the model is appropriate. These rendered images are just preliminary results and indicate perspectives for development in the research field of in situ measurements of the optical properties of snow. The image in

Figure 9 was rendered with the values estimated using Method 1, whereas the image in Figure 10 was rendered with the values estimated using Method 2.

Table 4. Values of the reduced scattering coefficients estimated from in situ reflectance profiles acquired with the TLS850 device.

Day	Method 1 μ_s' (mm^{-1})			Method 2 μ_s' (mm^{-1})		
	R	G	B	R	G	B
12	0.5153	0.5330	0.5182	0.4991	0.5186	0.5014
13	0.4641	0.4830	0.4547	0.4443	0.4612	0.4446
15	0.5058	0.5205	0.5106	0.4912	0.5057	0.4955
17	0.5134	0.5486	0.5254	0.4946	0.5305	0.5095
19	0.4142	0.4361	0.4186	0.4008	0.4208	0.4048
20	0.4659	0.4965	0.4721	0.4496	0.4784	0.4569
21	0.5038	0.5341	0.5181	0.4800	0.5085	0.4935
22	0.4398	0.4741	0.4508	0.4195	0.4531	0.4344
23	0.2779	0.2763	0.2854	0.2520	0.2521	0.2625
26	0.2976	0.3106	0.3098	0.2777	0.2866	0.2901
27	0.3359	0.3535	0.3537	0.3180	0.3310	0.3348
29	0.4199	0.4606	0.4261	0.4004	0.4405	0.4096
30	0.3673	0.3868	0.3798	0.3496	0.3656	0.3617
34	0.4390	0.5556	0.4988	0.4407	0.5362	0.4861

As can be observed, there are no significant differences in the appearance of these two images, although the values of the coefficients differ. There is potential to study acceptable variations of these coefficients for the rendering to remain convincing, and this would require subjective experiments. In the case of snow, the images we produced seem adapted, although some features could be added to make them more realistic. One could consider the bluish aspect of snow, as recent work has been conducted on rendering this aspect [2]. Studies have been conducted on modelling sparkle on materials [36,37]. Given the knowledge of sparkle we have shown, a physically based model of sparkle could be implemented and incorporated into rendered snow pictures.

Figure 9. Snow scene rendered using the values of the absorption and reduced scattering coefficients estimated with Method 1.

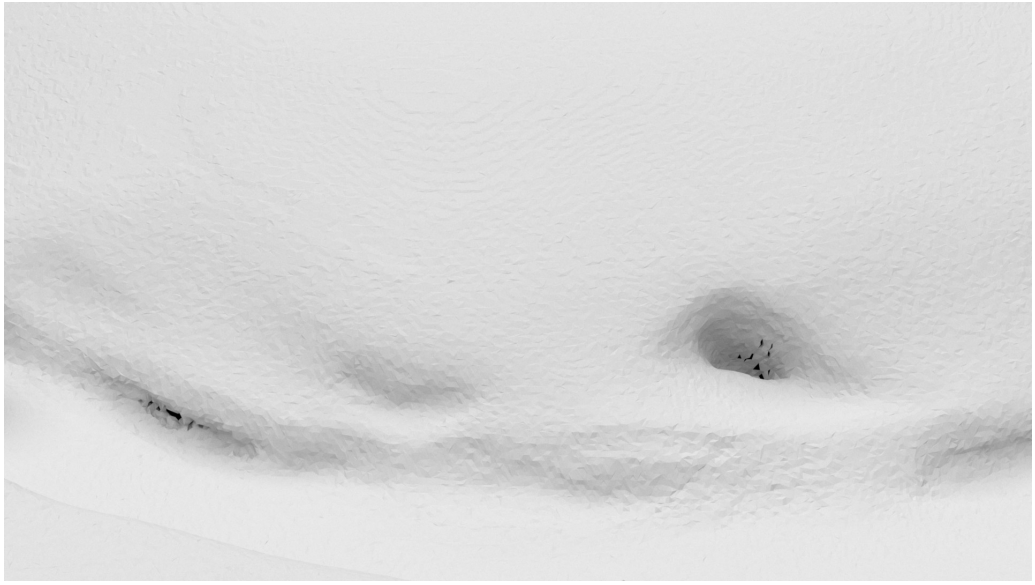

Figure 10. Snow scene rendered using the values of the absorption and reduced scattering coefficients estimated with Method 2.

4. Conclusions

We explored in situ measurement methods aimed at capturing and analysing physical correlates of the snow's visual appearance. In the case of the sparkle of snow, we were able to reproduce the measurement method with the new set of images. We obtained different results that do not allow us to conclude that sparkle could be used as a classification indicator for snow type. But it does not contradict it either. As it stands, it requires more attempts and shows that this type of study is difficult to conduct.

In the case of the absorption and scattering properties of snow, we were able to apply our measurement protocol and retrieve estimates of the absorption and reduced scattering coefficients. The estimates of μ_a in the case of snow were different from the theoretical values, but the data obtained by the device and the inversion method were developed for low-absorptive materials, thus making it difficult to obtain precise values for small quantities. By comparing the reduced scattering coefficients obtained from the two inversion methods, we can confirm that the absorption coefficients for snow can be neglected. We fed these measurements into a physically based renderer to generate simulated snow images. The results are preliminary and require improvements to make them appear more realistic.

5. Future Work

The first suggestion for future work on studying the sparkle of snow is to build a large database containing images of various types of snow from several locations worldwide, captured under different conditions and temperatures. The grain-type classification should be carried out by snow experts and by following a standardised nomenclature. This can be accomplished by measuring the grain size or measuring the specific surface area of snow grains [38]. Additionally, other parameters, such as the density, hardness, and wetness of the snow, could be recorded. This database could be combined with deep learning techniques to obtain the best possible results in the identification of snow. Furthermore, for the sparkle study in this paper, a daylight setup was mainly used. However, a nighttime setup with artificial lighting could also be used. Light sources could be controlled more efficiently, and the contrast on the snow would be increased due to the ambient darkness. Sparkle spots could thus be more frequent. Another suggestion for future investigation is to study the variations in temperature one or two hours before the capturing of sparkle events to check for a potential relationship between these variations and the sparkle indicators.

Finally, one could investigate the chromatic changes occurring on the sparkle of snow, which could be achieved in a nighttime setting where light is controlled.

Regarding the study of the absorption and scattering coefficients of snow, the rendered images could be used for simulations to confirm the estimated values we obtained with our inversion model. Ultimately, both methods we have explored in this study can be applied and allow coherent results. One could imagine incorporating the knowledge of these physical correlates into a rendering model of snow for virtual scenes. Another suggestion for future investigation is to look at spatial surveys of the snow sites and check for potential relationships between the physical correlates we have studied. Eventually, it would be interesting to explore if these methods could be used for cameras embedded in drones to remain in a close-range setup but perhaps cover a larger surface.

Author Contributions: The data curation, investigation, and writing of the original draft were conducted by M.N. All authors (i.e., M.N., J.-B.T. and I.F.) contributed equally to the conceptualisation, formal analysis, methodology, project administration, supervision, validation, and reviewing and editing of the draft. All authors have read and agreed to the published version of the manuscript.

Funding: This research received no external funding.

Data Availability Statement: Publicly available datasets were processed and analysed during this study. The data can be found at the following repository (accessed on 19 January 2024): https://github.com/MathieuNg/Data_Winter_2023.git.

Conflicts of Interest: The authors declare no conflict of interest.

References

1. Bohren, C.F. Colors of snow, frozen waterfalls, and icebergs. *J. Opt. Soc. Am.* **1983**, *73*, 1646–1652. [CrossRef]
2. Varsa, P.M.; Baranoski, G.V.G. Rendering the Bluish Appearance of Snow: When Light Transmission Matters. *IEEE Comput. Graph. Appl.* **2023**, 1–13. [CrossRef] [PubMed]
3. Flanner, M.G.; Zender, C.S. Linking snowpack microphysics and albedo evolution. *J. Geophys. Res. Atmos.* **2006**, *111*, 320. [CrossRef]
4. Aoki, T.; Kuchiki, K.; Niwano, M.; Kodama, Y.; Hosaka, M.; Tanaka, T. Physically based snow albedo model for calculating broadband albedos and the solar heating profile in snowpack for general circulation models. *J. Geophys. Res. Atmos.* **2011**, *116*, 140. [CrossRef]
5. Pointer, M.R. *Measuring Visual Appearance—A Framework of the Future*; Project 2.3 Measurement of Appearance; NPL Report COAM 19; National Physical Laboratory: London, UK, 2003.
6. Fierz, C.; Armstrong, R.L.; Durand, Y.; Etchevers, P.; Greene, E.; McClung, D.M.; Nishimura, K.; Satyawali, P.K.; Sokratov, S.A. *The International Classification of Seasonal Snow on the Ground*; UNESCO-IHP Technical Report; UNESCO: Paris, France, 2009.
7. Kokhanovsky, A.A.; Zege, E.P. Scattering optics of snow. *Appl. Opt.* **2004**, *43*, 1589–1602. [CrossRef] [PubMed]
8. Nakaya, U. *Snow Crystals: Natural and Artificial*; Harvard University Press: Cambridge, MA, USA, 1954. [CrossRef]
9. Pirazzini, R. Surface albedo measurements over Antarctic sites in summer. *J. Geophys. Res. Atmos.* **2004**, *109*, 97. [CrossRef]
10. Pirazzini, R.; Räisänen, P.; Vihma, T.; Johansson, M.; Tastula, E.M. Measurements and modelling of snow particle size and shortwave infrared albedo over a melting Antarctic ice sheet. *Cryosphere* **2015**, *9*, 2357–2381. [CrossRef]
11. Kokhanovsky, A.A.; Breon, F.M. Validation of an Analytical Snow BRDF Model Using PARASOL Multi-Angular and Multispectral Observations. *IEEE Geosci. Remote Sens. Lett.* **2012**, *9*, 928–932. [CrossRef]
12. Pirazzini, R.; Leppänen, L.; Picard, G.; Lopez-Moreno, J.I.; Marty, C.; Macelloni, G.; Kontu, A.; Von Lerber, A.; Tanis, C.M.; Schneebeli, M.; et al. European in-situ snow measurements: Practices and purposes. *Sensors* **2018**, *18*, 2016. [CrossRef]
13. Frisvad, J.R.; Jensen, S.A.; Madsen, J.S.; Correia, A.; Yang, L.; Gregersen, S.K.S.; Meuret, Y.; Hansen, P.E. Survey of Models for Acquiring the Optical Properties of Translucent Materials. *Comput. Graph. Forum* **2020**, *39*, 729–755. [CrossRef]
14. Chandrasekhar, S. *Radiative Transfer*; Dover Publications: New York, NY, USA, 2013.
15. Nicodemus, F.E.; Richmond, J.C.; Hsia, J.J.; Ginsberg, I.W.; Limperis, T. *Geometrical Considerations and Nomenclature for Reflectance*; National Bureau of Standards: Gaithersburg, MD, USA, 1977.
16. Guarnera, G.C.; Ghosh, A.; Hall, I.; Glencross, M.; Guarnera, D. Material Capture and Representation with Applications in Virtual Reality. In Proceedings of the ACM SIGGRAPH 2017 Courses, Association for Computing Machinery (SIGGRAPH '17), Los Angeles, CA, USA, 30 July–3 August 2017. [CrossRef]
17. Wiscombe, W.J.; Warren, S.G. A Model for the Spectral Albedo of Snow. I: Pure Snow. *J. Atmos. Sci.* **1980**, *37*, 2712–2733. [CrossRef]
18. Libois, Q.; Picard, G.; France, J.L.; Arnaud, L.; Dumont, M.; Carmagnola, C.M.; King, M.D. Influence of grain shape on light penetration in snow. *Cryosphere* **2013**, *7*, 1803–1818. [CrossRef]

19. Picard, G.; Arnaud, L.; Domine, F.; Fily, M. Determining snow specific surface area from near-infrared reflectance measurements: Numerical study of the influence of grain shape. *Cold Reg. Sci. Technol.* **2009**, *56*, 10–17. [CrossRef]
20. Jensen, H.W.; Marschner, S.R.; Levoy, M.; Hanrahan, P. A Practical Model for Subsurface Light Transport. In Proceedings of the 28th Annual Conference on Computer Graphics and Interactive Techniques, Association for Computing Machinery (SIGGRAPH '01), New York, NY, USA, 1 August 2001; pp. 511–518. [CrossRef]
21. Donner, C.; Lawrence, J.; Ramamoorthi, R.; Hachisuka, T.; Jensen, H.W.; Nayar, S. An Empirical BSSRDF Model. *ACM Trans. Graph.* **2009**, *28*, 10. [CrossRef]
22. Warren, S.G. Optical constants of ice from the ultraviolet to the microwave. *Appl. Opt.* **1984**, *23*, 1206–1225. [CrossRef] [PubMed]
23. Picard, G.; Libois, Q.; Arnaud, L. Refinement of the ice absorption spectrum in the visible using radiance profile measurements in Antarctic snow. *Cryosphere* **2016**, *10*, 2655–2672. [CrossRef]
24. Warren, S.G.; Brandt, R.E. Optical constants of ice from the ultraviolet to the microwave: A revised compilation. *J. Geophys. Res. Atmos.* **2008**, *113*, 786. [CrossRef]
25. Nguyen, M.; Thomas, J.B.; Farup, I. Measuring the Optical Properties of Highly Diffuse Materials. *Sensors* **2023**, *23*, 6853. [CrossRef]
26. Kirchner, E.; van der Lans, I.; Perales, E.; Martínez-Verdú, F.; Campos, J.; Ferrero, A. Visibility of sparkle in metallic paints. *J. Opt. Soc. Am. A* **2015**, *32*, 921–927. [CrossRef]
27. Nguyen, M.; Thomas, J.B.; Farup, I. Statistical Analysis of Sparkle in Snow Images. *J. Imaging Sci. Technol.* **2022**, *66*, 050404. [CrossRef]
28. Ferrero, A.; Bayón, S. The measurement of sparkle. *Metrologia* **2015**, *52*, 317. [CrossRef]
29. Avanzi, F.; Hirashima, H.; Yamaguchi, S.; Katsushima, T.; De Michele, C. Observations of capillary barriers and preferential flow in layered snow during cold laboratory experiments. *Cryosphere* **2016**, *10*, 2013–2026. [CrossRef]
30. Nguyen, M.; Thomas, J.B.; Farup, I. Investigating the Kokhanovsky snow reflectance model in close range spectral imaging. In Proceedings of the 29th Color and Imaging Conference (CIC 2021), Online, 1–15 November 2021; pp. 31–36. [CrossRef]
31. Montpetit, B.; Royer, A.; Langlois, A.; Chum, M.; Cliche, P.; Roy, A.; Champollion, N.; Picard, G.; Dominé, F.; Obbard, R. In-situ Measurements for Snow Grain Size and Shape Characterization Using Optical Methods. In Proceedings of the 68th Annual Eastern Snow Conference, Montreal, QC, Canada, 14–16 June 2011; pp. 173–188.
32. Farrell, T.J.; Patterson, M.S.; Wilson, B. A diffusion theory model of spatially resolved, steady-state diffuse reflectance for the noninvasive determination of tissue optical properties in vivo. *Med. Phys.* **1992**, *19*, 879–888. [CrossRef]
33. Website Tracking Temperatures in Norway. Available online: https://www.yr.no/en (accessed on 22 January 2024).
34. Leppänen, L.; Kontu, A.; Vehviläinen, J.; Lemmetyinen, J.; Pulliainen, J. Comparison of traditional and optical grain-size field measurements with SNOWPACK simulations in a taiga snowpack. *J. Glaciol.* **2015**, *61*, 151–162. [CrossRef]
35. Jakob, W.; Speierer, S.; Roussel, N.; Nimier-David, M.; Vicini, D.; Zeltner, T.; Nicolet, B.; Crespo, M.; Leroy, V.; Zhang, Z. Mitsuba 3 Renderer. 2022. Available online: https://mitsuba-renderer.org (accessed on 22 January 2024).
36. Jakob, W.; Hašan, M.; Yan, L.Q.; Lawrence, J.; Ramamoorthi, R.; Marschner, S. Discrete Stochastic Microfacet Models. *ACM Trans. Graph.* **2014**, *33*, 115. [CrossRef]
37. Wang, B.; Bowles, H. A Robust and Flexible Real-Time Sparkle Effect. In Proceedings of the Eurographics Symposium on Rendering: Experimental Ideas & Implementations, Dublin, Ireland, 22–24 June 2016; Eurographics Association: Goslar, Germany, 2016; pp. 49–54.
38. Martin, J.; Schneebeli, M. Impact of the sampling procedure on the specific surface area of snow measurements with the IceCube. *Cryosphere* **2023**, *17*, 1723–1734. [CrossRef]